PCCP

Accepted Manuscript

ROYAL SOCIETY OF CHEMISTRY

www.rsc.org/pccp

PCCP

RSCPublishing

PAPER

Energetics and Structural Evolution of Na - Ca Exchanged Zeolite A during Heating

Cite this: DOI: 10.1039/x0xx00000x

H. Sun,[a] D. Wu,[b] X. Guo,[b] and A. Navrotsky *[b]

Received 00th September 2014,
Accepted 00th September 2014

DOI: 10.1039/x0xx00000x

www.rsc.org/

The properties of zeolite A change significantly with sodium – calcium exchange. The impact of cation composition on the temperature – induced phase transformations and energetics for Na – Ca exchanged zeolite A was studied systematically using powder X-ray diffraction (XRD), thermogravimetric analysis (TGA), differential scanning calorimetry (DSC) and high-temperature oxide melt solution calorimetry. As the temperature increases, the structural evolution of each Na – Ca exchanged zeolite A undergoes three distinct stages, dehydration, amorphization, and densification/recrystallization. Complete dehydration does not initially result in framework degradation, but further heating leads to zeolite phase degradation into other aluminosilicate phases. Both amorphization and recrystallization shift to higher temperatures as the calcium content. On the other hand, the enthalpies of formation for the high temperature aluminosilicate phases, amorphous (AP) and dense phase (DP), appear to be linear functions of calcium content (average ionic potential) with energetic stability diminishing with increasing Ca content. 100 % Na-A heated at 1200 ^{o}C has the most exothermic formation enthalpy from oxides (-65.87 ± 0.87 kJ/mol - TO_2), while 97.9 % Ca Na-A heated at 945 ^{o}C has the least exothermic (-5.26 ± 0.62 kJ/mol - TO_2). For different aluminosilicates with the same chemical composition, the dense phase assemblage (DP) is more stable than the amorphous (AP).

1. Introduction

Zeolites have well-defined framework structures and exchangeable extra-framework cations. They usually feature a large internal area/volume ratio as well as tunable aperture sizes. These unique properties lay the foundation for their excellent adsorption and catalytic properties. Development of inorganic synthesis techniques in the last several decades has brought us numerous synthetic zeolite structures, including cation-exchanged analogues and modified forms, which have been employed in a wide range of industrial applications, including catalysis, ion exchange and selective adsorption [1-4]. However, regardless of the details of structure, zeolites usually suffer from framework degradation at elevated temperature, in which the pores are destroyed, the three-dimensional structures collapse, and either amorphous phases (AP) or dense crystalline phases (DP) such as quartz. Hence, knowledge of the temperature-induced phase transformation details is very important for optimizing zeolite applications and avoiding permanent deactivation of catalysts or decreased sorption capacity. On the other hand, zeolites may also serve as precursors in fabrication of novel dense solid state materials such as glass, ceramics and electrolytes [5-7], in which their versatile open structures offer great simplicity for uniform compositional modification. This provides another motivation for investigating the thermal and thermodynamic responses of doped or precursor-filled zeolites upon heating.

Phase transformation of porous materials during heating originates directly from their intrinsic metastability. Though hydrated aluminoslicate zeolites can be thermodynamically stable at low temperatures, their dehydrated forms are generally metastable with respect to dense phase mineral assemblages. Therefore, running downhill in free energy, structure degradations involving amorphization, recrystallization and/or other phase transitions are commonly observed, especially upon exposure to heating in air or hydrothermal conditions [8-11]. Moreover, the charge-balancing cations bring additional degrees of freedom, directing the formation of different phases at high temperature. Hence, knowing the underlying relations among cation content, phase transformation, and energetics of various intermediate and final products is very important for optimizing the development and application of zeolites.

Thermal and thermodynamic stability and transformation of zeolites have attracted extensive interest [12-14], in which the impacts of multiple factors have been investigated systematically [15-18]. Other than the framework topology, Si/Al ratio and type of thermal treatment, it has been emphasized that the extra-framework guest species, such as metal cations and/or H_2O molecules, have significant impact on stability and phase evolution. The stable phase assemblage at a given composition is determined by thermodynamic equilibrium, while the transformation pathway is governed by kinetic factors.

Due to its widespread applications in industrial processes including separation, purification, acid catalysis and material fabrication, zeolite A (see Figure 1) receives special attention from both scientific and engineering viewpoints[19-22]. Although phase evolution on heating NaA has been investigated by isothermal and non-isothermal methods [23, 24], the phase evolution and energetics of Ca-exchanged zeolite A as a function of calcium content and temperature, have not been studied. Here, we employ thermogravimetric analysis (TGA) and differential scanning calorimetry (DSC) to investigate the temperature derived phase transition (up to 1200 ^{o}C) of a series of Ca – Na exchanged zeolite A samples as a function of calcium content. Energetics of the amorphous, intermediate and final dense aluminosilicate phases

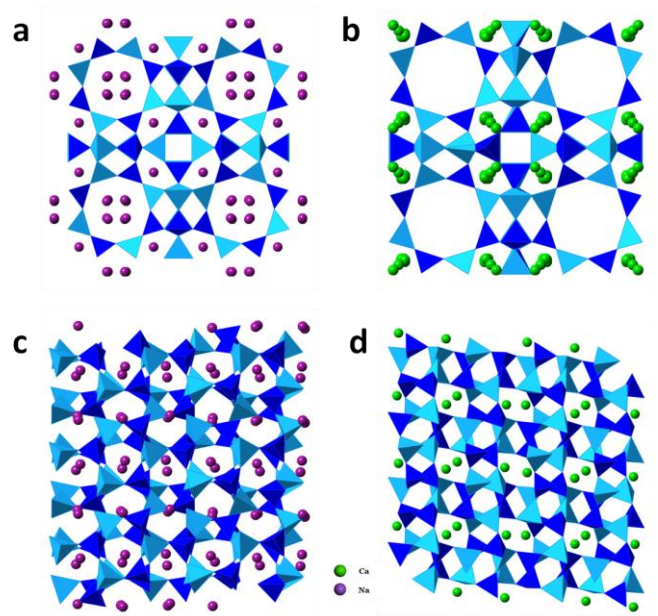

Figure 1. Crystal structures of zeolite Na-A (a), zeolite Ca-A (b), nepheline (c), and anorthite (d). Tetrahedra represent AlO_4 or SiO_4.

were determined by high temperature oxide melt solution calorimetry. We explore the complex composition – phase – energetics relations as a function of temperature in order to better understand the thermodynamic driving forces for the observed transformations.

2. Experimental methods

2.1. Material preparation

Synthetic zeolite Na-A (RM 8851) obtained from the National Institute of Standards and Technology (NIST) was used as starting material. All zeolite CaNa-A samples were prepared by calcium ion-exchange, in which 2.0 g Na-A was suspended into 40 ml $CaCl_2$ aqueous solution (0.05 to 0.25 M) and ion-exchanged under constant stirring at 80 °C for 24 hours. Then, the solid product was separated by centrifugation and washed at least three times with deionized water. The above ion-exchange procedure was triplicated to maximize degree of Ca-exchange. The solid products were then dried at 120 °C overnight, and equilibrated in a tightly sealed desiccator with 33 ± 2 % relative humidity generated from saturated aqueous $MgCl_2$ solution for at least two days.

2.2. Characterization

TGA-DSC was performed on a Netzsch STA 449 system. The heating rate may have great impact on the DSC curve. A faster heating rate magnifies the thermal effects, yet can also bury kinetic details. According to our experimental experience on numerous thermal analyses of zeolite materials, a moderate heating rate is usually optimal. For the current case we use 10 K/min. A sample weighing about 20 mg was placed in a platinum crucible and heated from room temperature to various final temperatures (905, 945 and 1200 °C) at 10 °C/min under argon flow (40 ml/min). Upon the end of the heating program, the samples were quenched under argon flow. Then the treated sample was collected for further structural characterization and calorimetry.

The structure and phase evolution to different temperatures was explored using powder X-ray diffraction (XRD) performed on a Bruker-AXS D8 Advance X-ray diffractometer operated at 40 kV and 40 mA with Cu Kα radiation. Data were recorded from 5 to 60 ° (2θ) with a step size of 0.02 ° (1 s·step^{-1}). All the XRD patterns were refined by Jade 6.0 and ICSD database.

Chemical compositions were analyzed using a Cameca SX-100 electron microprobe with a beam current of 10 nA and an accelerating voltage of 15 kV. Eight points were measured at various positions on each specimen. The sample homogeneity was confirmed using backscattered electron imaging.

2.3. Calorimetry

High-temperature oxide melt solution calorimetry was performed in a custom-built Tian – Calvet twin microcalorimeter. The methodology has been described in detail by Navrotsky [25, 26]. Molten lead borate ($2PbO{\cdot}B_2O_3$) at 704 °C was used as the solvent. Prior to calorimetry, each sample was heated gradually to 450 °C and degassed for 16 h under vacuum (10^{-4} torr) on an ASAP 2020 gas adsorption analyzer. This fully dehydrated sample was hand-pressed into a pellet (about 5 mg) and dropped from ambient into the calorimeter containing the solvent under argon flow (100 ml/min). The measurement was repeated at least five times to ensure reproducibility. The calorimeter was calibrated using the heat content of corundum.

3. Results

3.1. Chemical composition

The chemical composition and molar mass (TO_2 basis) of dehydrated and hydrated zeolites A are listed in Table 1. All samples have identical Si/Al ratio (1.03 ± 0.01), which is very close to that (1.00) of the ideal zeolite A framework. The degree of Ca-exchange ranges from 34.8 to 97.9 %.

3.2. Thermogravimetric analysis and differential scanning calorimetry (TG-DSC)

TGA profiles represent the dehydration process of hydrated zeolite A samples. The number of water molecules per pseudo unit cell (48 oxygen formula) are calculated from weight loss and plotted in Figure 2. The exact water content per TO_2 unit is listed in Table 1.
The DSC traces for all zeolite A samples are presented in Figure 3. Phase transformations take place at 800 to 1200 °C. Pure zeolite Na-A merely has a single exothermic peak at 898 °C. However, three distinct exothermic heat events (883, 922 and 976 °C, labeled as Peak I, Peak II and Peak III in Table 2), which are consistent with

Table 1. Chemical compositions of hydrated and dehydrated zeolites Na-A and CaNa-A (on TO_2 basis).

Sample	Composition	MW_{hyd} (g)	MW_{deh} (g)
Na-A	$Na_{0.481}Al_{0.493}Si_{0.510}O_2{\cdot}1.014H_2O$	88.95	70.68
34.8%CaNa-A[a]	$Na_{0.299}Ca_{0.080}Al_{0.495}Si_{0.514}O_2{\cdot}1.083H_2O$	89.38	69.87
44.5%CaNa-A[a]	$Na_{0.285}Ca_{0.115}Al_{0.491}Si_{0.503}O_2{\cdot}1.100H_2O$	90.34	70.53
63.0%CaNa-A[a]	$Na_{0.182}Ca_{0.154}Al_{0.498}Si_{0.504}O_2{\cdot}1.140H_2O$	90.49	69.94
76.2%CaNa-A[a]	$Na_{0.121}Ca_{0.193}Al_{0.487}Si_{0.508}O_2{\cdot}1.152H_2O$	90.68	69.92
97.9%CaNa-A[a]	$Na_{0.011}Ca_{0.248}Al_{0.487}Si_{0.508}O_2{\cdot}1.204H_2O$	91.30	69.60

[a] The values in front of *CaNa-A* denote the degrees of calcium exchange of CaNa-A samples.

Table 2. Positions of exothermic peaks and heat of phase transition from integration of DSC exothermic peaks (see Figure 3).

Sample	T_{max}(°C)			ΔH_{int} [a] (kJ/mol)		
	Peak I	Peak II	Peak III	Peak I	Peak II	Peak III
Na-A	N/A	N/A	898.0	N/A	N/A	-10.65 ± 0.47 (3) [b]
34.8%CaNa-A	883.0	922.4	976.4	-3.88 ± 0.30 (4) [b]	-7.69 ± 0.33 (4) [b]	-8.21 ± 0.37 (3) [b]
44.5%CaNa-A	891.5	979.5	990.5	-6.56 ± 0.65 (3) [b]	N/A	-19.75 ± 0.57 (3) [b]
63.0%CaNa-A	901.2	978.2	1010.2	-6.95 ± 1.13 (3) [b]	N/A	-20.43 ± 1.23 (3) [b]
76.2%CaNa-A	905.2	980.2	1017.2	-9.11 (1) [b]	N/A	-25.58 (1) [b]
97.9%CaNa-A	934.6	N/A	1020.6	-12.04 (2) [b]	N/A	-25.67 (2) [b]

[a] Integrated heats of phase transition.
[b] The values in parentheses denote the number of measurements.

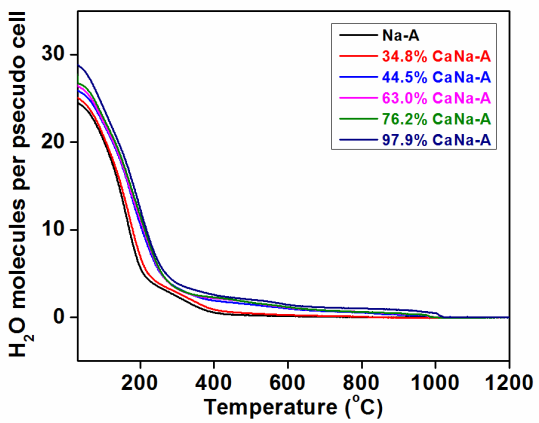

Figure 2. TGA traces for hydrated zeolites Na-A and CaNa-A.

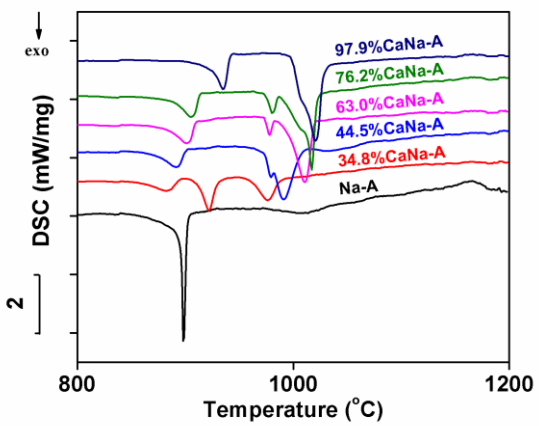

Figure 3. DSC profiles for hydrated zeolites Na-A and CaNa-A. The exothermic direction is shown by an arrow.

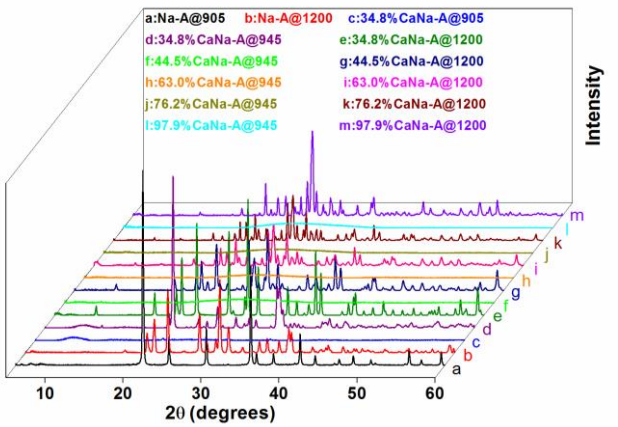

Figure 4. XRD patterns for amorphous phases (AP), intermediate phases (IP), and dense phases (DP) of calcium - sodium exchanged zeolite A.

those of nepheline (880, 920 and 990 °C) [27], are observed for zeolite 34.8% CaNa-A. As the calcium content continue increasing, Peak I sharpens and shifts to higher temperatures (883 °C for 34.8 % CaNa-A and 935 °C for 97.9 % CaNa-A). On the other hand, Peak II shifts to a fixed temperature (~980 °C) and becomes better resolved as Peak III shifts to higher temperature (991 °C for 44.5 % CaNa-A and 1017 °C for 76.2 % CaNa-A). For the nearly fully exchanged Ca-exchanged sample (97.9 % CaNa-A), Peak II entirely merges with Peak III, which then appears to be asymmetric, having a shoulder on the lower temperature side. The magnitude for all heat events was calculated by integration of each DSC peak (see Table 2).

3.3. X-ray diffraction

The powder XRD patterns, including starting zeolite A materials and post thermal treatment phases are presented in Figure 4, which illustrates the phase transformation details as a function of calcium content and temperature. According to the position of DSC peaks, we collected XRD patterns for samples quenched from 905, 945 and 1200 °C. Specifically, Na-A@905 has a low-temperature carnegieite structure [17]. 34.8 % CaNa-A becomes amorphous at 905 °C. All the other Ca-exchanged zeolites exhibit

Table 3. Thermodynamic cycles for formation enthalpies of dehydrated calcium - sodium exchanged aluminosilicates from oxides.
ΔH_1 and ΔH_6 are the drop solution enthalpies of calcium - sodium exchanged aluminosilicates; ΔH_2, ΔH_3, ΔH_4, and ΔH_7 are the drop solution enthalpies of oxides; ΔH_5 and ΔH_8 are the formation enthalpies of aluminosilicates from oxides.

Enthalpy of formation of sodium aluminosilicates	
$x/2Na_2O$ (soln., 704 °C) + $y/2Al_2O_3$ (soln., 704 °C) + $zSiO_2$ (soln., 704 °C) → $Na_xAl_ySi_zO_2$ (s, 25 °C)	$\Delta H_1 = \Delta H_{ds\text{-}deh}$
Na_2O (s, 25 °C) → Na_2O (soln., 704 °C)	ΔH_2
Al_2O_3 (s, 25 °C) → Al_2O_3 (soln., 704 °C)	ΔH_3
SiO_2 (s, 25 °C) → SiO_2 (soln., 704 °C)	ΔH_4
$x/2Na_2O$ (s., 25 °C) + $y/2Al_2O_3$ (s., 25 °C) + $zSiO_2$ (s., 25 °C) → $Na_xAl_ySi_zO_2$ (s, 25 °C)	$\Delta H_5 = \Delta H_{f\text{-}deh,ox}$
$\Delta H_5 = \Delta H_1 + x/2\Delta H_2 + y/2\Delta H_3 + z\Delta H_4$	
Enthalpy of formation of Ca-Na exchanged aluminosilicates	
$a/2Na_2O$ (soln., 704 °C) + $bCaO$ (soln., 704 °C) + $c/2Al_2O_3$ (soln., 704 °C) + $dSiO_2$ (soln., 704 °C) → $Na_aCa_bAl_cSi_dO_2$ (s, 25 °C)	$\Delta H_6 = \Delta H_{ds\text{-}deh}$
Na_2O (s, 25 °C) → Na_2O (soln., 704 °C)	ΔH_2
Al_2O_3 (s, 25 °C) → Al_2O_3 (soln., 704 °C)	ΔH_3
SiO_2 (s, 25 °C) → SiO_2 (soln., 704 °C)	ΔH_4
CaO (s, 25 °C) → CaO (soln., 704 °C)	ΔH_7
$a/2Na_2O$ (s, 25 °C) + $bCaO$ (s, 25 °C) + $c/2Al_2O_3$ (s, 25 °C) + $dSiO_2$ (s, 25 °C) → $Na_aCa_bAl_cSi_dO_2$ (s, 25 °C)	$\Delta H_8 = \Delta H_{f\text{-}deh,ox}$
$\Delta H_8 = \Delta H_6 + a/2\Delta H_2 + c/2\Delta H_3 + d\Delta H_4 + b\Delta H_7$	

Table 4. Drop solution enthalpies for constituent oxides in molten lead borate at 704 °C (on the basis of mole TO_2).

Sample	ΔH_{ds} (kJ/mol)
Sodium oxide (Na_2O)	-113.10 ± 0.83[a]
Calcium oxide (CaO)	-17.49 ± 1.21[a]
Corundum (Al_2O_3)	-107.93 ± 0.98[a]
Quartz (SiO_2)	39.13 ± 0.32[a]

[a] Ref. [34].

structural collapse leading to amorphous phases (AP) after heating to 945 °C. After Peak II, 34.8 % CaNa-A@945 is confirmed to be carnegieite [27]; here we call it an intermediate phase (IP). All samples transform to dense phases (DP) upon to 1200 °C. XRD refinement suggests that Na-A@1200, 34.8 % CaNa-A@1200 and 97.9 % CaNa-A@1200 are pure sodium nepheline (Na-NEP), nepheline (NEP) and anorthite (ANO), respectively (see Figure 1). For the other three CaNa-A samples, heating results in phase transformation and phase separation. Their corresponding dense phases are mixtures of NEP and ANO. The phase compositions (in mass fraction) are (68.3 ± 0.3) % NEP + (31.2 ± 0.2) % ANO for 44.5 % CaNa-A@1200, (47.7 ± 0.2) % NEP + (52.3 ± 0.2) % ANO for 63.0 % CaNa-A@1200 and (40.1 ± 0.2) % NEP + (59.9 ± 0.3) % ANO for 76.2 % CaNa-A@1200. For samples having more than 34.5 % calcium, the intermediate phase assemblage cannot be separated for XRD analysis as Peaks II and III are very close in temperature.

3.4. High-temperature oxide melt drop solution calorimetry

Using the thermodynamic cycles in Table 3, the enthalpy of formation (at 25 °C) of each phase from constituent oxides ($\Delta H_{f,ox}$) was calculated from the drop solution enthalpy of the dehydrated sample ($\Delta H_{ds\text{-}deh}$). ΔH_{ds} values of constituent oxides used for the thermodynamic calculation are listed in Table 4. The calculated formation enthalpies from oxides are presented in Table 5. The formation enthalpies of anhydrous zeolites (AZ) are also listed in Table 6 for comparison [28]. For samples with the same composition, the formation enthalpies of amorphous phases (AP) are less exothermic than those of dense phases (DP). The enthalpies of formation for both AP and DP become less exothermic as the degree of Ca-exchange increases. The dense phase Na-A@1200 has the most exothermic formation enthalpy of -65.87 ± 0.87 kJ/mol - TO_2 while the amorphous phase 97.9%CaNa-A@945 presents the least exothermic value, -5.26 ± 0.62 kJ/mol - TO_2. Na-A@905 has a very similar formation enthalpy (-64.71 ± 0.93 kJ/mol - TO_2) to that of Na-A@1200,

Table 5. Enthalpies of drop solution and formation (25 °C) of AZ, AP, IP, and DP of calcium - sodium exchanged aluminosilicates (on mole TO_2 basis).

Sample	$\Delta H_{ds\text{-}deh}$[a] (kJ/mol)	$\Delta H_{f,ox}$[b] (kJ/mol)
Na-A		-42.20±1.21[d]
Na-A@905	83.98±0.86 (6)[c]	-64.71±0.93
Na-A@1200	85.14±0.79 (5)[c]	-65.87±0.87
34.8%CaNa-A		-29.54±1.28[d]
34.8%CaNa-A@905	61.40±0.67 (6)[c]	-33.15±0.74
34.8%CaNa-A@945	69.48±0.70 (6)[c]	-41.24±0.77
34.8%CaNa-A@1200	78.18±0.55 (5)[c]	-49.93±0.64
44.5%CaNa-A		-25.61±1.54[d]
44.5%CaNa-A@945	57.87±0.61 (6)[c]	-29.65±0.69
44.5%CaNa-A@1200	74.92±0.63 (5)[c]	-46.70±0.71
63.0%CaNa-A		-17.51±1.22[d]
63.0%CaNa-A@945	52.14±0.37 (5)[c]	-18.62±0.50
63.0%CaNa-A@1200	70.74±0.81 (6)[c]	-37.22±0.87
76.2%CaNa-A		-17.72±1.76[d]
76.2%CaNa-A@945	50.44±0.47 (5)[c]	-14.30±0.58
76.2%CaNa-A@1200	69.45±0.63 (6)[c]	-33.31±0.72
97.9%CaNa-A		-5.94±1.64[d]
97.9%CaNa-A@945	46.68±0.50 (5)[c]	-5.26±0.62
97.9%CaNa-A@1200	64.51±0.53 (6)[c]	-23.08±0.64

[a] Drop solution enthalpy of samples.
[b] Formation enthalpy of samples from oxides.
[c] The values in parentheses denote the number of measurements.
[d] The values of formation enthalpy for dehydrated zeolites are obtained from ref [28].

which corresponds to the DSC profile which shows no detectable thermal events in the transition from carnegieite (IP) to nepheline (DP). In addition, the enthalpies of formation of Na-A@1200 (-65.87 ± 0.87 kJ/mol - TO_2) and 97.9 % CaNa-A@1200 (-23.08 ± 0.64 kJ/mol - TO_2) are in good accordance with previously reported enthalpies of formation of pure sodium nepheline (-67.20 ± 2.04 kJ/mol - TO_2) and anorthite (-25.45 ± 0.79 kJ/mol - TO_2) [29]. Such similarity strongly supports our phase identification from structural refinement. The slight variation in enthalpy may originate from small compositional differences.

4. Discussion

In practical applications, the thermodynamic properties of zeolites at high temperature are needed for optimizing performance. The present work demonstrates possible compositional and structural transitions that zeolites may undergo during heating. In particular, the changes in Ca-Na exchanged zeolite A occur in three distinct steps as a function of temperature: dehydration, amorphization, and recrystallization to dense phases [13]. Previous studies suggest that the phase transition can be significantly impacted by the chemical compositions of zeolite A, both the degree of Al substitution, and cation type/content [17, 27]. With identical Al content for all samples, our study highlights the dominant role of calcium – sodium substitution.

The first event associated with heating these zeolites from room temperature is dehydration. This process is endothermic in enthalpy but positive in entropy because of the release of gaseous H_2O and it thus becomes favorable at high temperature. In the case of zeolite A, the dehydrated zeolite framework, though metastable with respect to dense phases, persists over a large temperature range.

As the temperature approaches 900 ^oC, zeolite A loses its long range order while preserving short range order around each tetrahedral atom (Al or Si). Particularly, the Al-O-Si bridges break, followed by framework collapses into disordered arrangements of tetrahedral building blocks (AlO_4 or SiO_4) that are still largely linked to form a more dense but random distribution of rings without the organized large pores and channels characteristic of the initial zeolite structure [17]. As a result, the zeolitic structure becomes amorphous. For 34.8 % CaNa-A the amorphization takes place at slightly below 900 ^oC (Peak I in Figure 3 and Table 2). It then shifts to higher temperature (up to 935 ^oC for 97.9 % CaNa-A) as the mole fraction of calcium or average ionic potential (Z/r, is the ratio of average charge to the average radius of a mixture of ions) increases. Similar order-disorder transitions are also observed in the calcination of as-made, structural-directing agent (SDA)

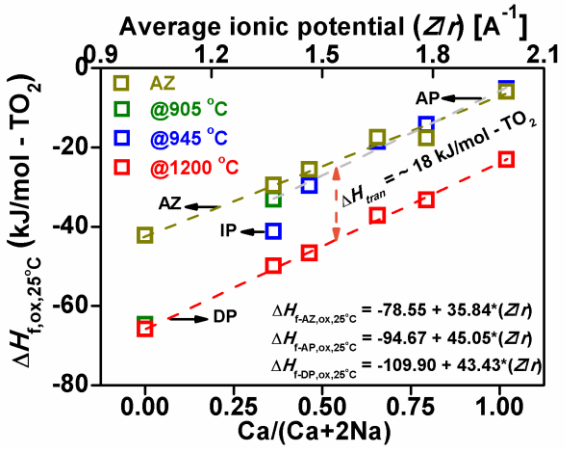

Figure 5. Formation enthalpies from binary oxides of AZ, AP, IP, and DP of calcium - sodium exchanged zeolite A from oxides (per mole TO_2) versus mole fraction of calcium and average ionic potential. Points denote the measured results and dashed lines show the linear fitting. $\Delta H_{f\text{-}AZ,\ ox,\ 25\ ^oC}$, $\Delta H_{f\text{-}AP,\ ox,\ 25\ ^oC}$ and $\Delta H_{f\text{-}DP,\ ox,\ 25\ ^oC}$ are the formation enthalpies of AZ, AP and DP relative to constituent oxides at 25 °C. ΔH_{tran} is the enthalpy for the phase transition from AP to DP.

containing zeolites, in which removing the embedded SDA may lead to framework amorphization [30]. Although the kinetic details for these two types of amorphization vary, they all highlight the intrinsic metastability of anhydrous and SDA free zeolites.

The final step for calcination of Ca-Na exchanged zeolite A is densification/recrystallization. Overcoming kinetic energy barriers on heating the disordered tetrahedra reassemble to new, more stable, dense crystalline aluminosilicates, as supported by the formation enthalpy data as well as previous studies [29]. Zeolites Na-A and Ca-A eventually transform into nepheline and anorthite, respectively. All the other partially Ca-exchanged zeolites A samples form mixtures of nepheline and anorthite. The increase in phase transition temperature with Ca-content is also observed in the densification process (center of DSC peak III in Figure 3). In addition, thermal treatment of zeolite A may also lead to intermediate phases, such as the carnegieite structures observed for Na-A@905 and CaNa-A@945. Interestingly, unlike zeolite Ca-A, either DSC (Figure 3) or XRD (Figure 4) hint corresponding to AP formation is detected during thermal treatment of zeolite Na-A. A similar result has been reported previously [17]. This implies that the enthalpy of such transitions is small, as supported by the formation enthalpy data of different phases (see Figure 5). Moreover, the energetics also demonstrates a well-defined example of the Ostwald step rule, showing that the least stable phase (AP or IP) nearest to the original phase, AZ, usually appears ahead of the energetically most stable phase (DP), as seen in both solution systems [31] and natural mineralogical environments [32].

The enthalpies of formation for AP and DP become less exothermic as the average ionic potential or calcium content increases (see Figure 5), suggesting similar effects of ion exchange on the overall energetics for both classes of aluminosilicate phases. Similar compositional dependence is also found in previous studies on a variety of anhydrous aluminosilicates [29, 33]. These systematic trends suggest that the complex energetics of zeolite and their amorphous and dense phase products are governed primarily by the fundamental acid – base chemistry of ternary oxide formation. Specifically, the substitution of Si^{4+} with Al^{3+} and charge-compensating cations in zeolite structures ($Si^{4+} = Al^{3+} + 1/z\ M^{z+}$, in our case, $M^{z+} = Na^+$ or Ca^{2+}), depends on the basicity of the extra-framework cation. The enthalpy of formation becomes more exothermic as the basicity increases or the average ionic potential of the guest cation decreases. Such effects are observed not only for the zeolitic structures, but also for the amorphous and dense phases. The slopes of the variation of $\Delta H_{f,ox}$ with Ca content for AP and DP are nearly the same. For samples with the same composition, AP have less exothermic enthalpies of formation than DP, with a nearly constant difference of about 18 kJ/mol - TO_2. Such intrinisic differences in energetics provide the thermodynamic driving force for structural evolution of Ca-Na exchanged zeolite A during heating.

5. Conclusions

Zeolites CaNa-A with calcium contents ranging from 0 to 97.9 % were prepared and their energetics of phase transformation were investigated using XRD, TG-DSC and high-temperature oxide melt solution calorimetry. Several different stages of structural evolution as a function of degree of Ca-exchange and temperature were seen: dehydration, amorphization, and densification/recrystallization. The temperature for both amorphization and densification/recrystallization increases as the calcium content increases. The enthalpies of formation from binary oxides of the dehydrated zeolites, amorphous and dense aluminosilicates are all exothermic. For each phase, the enthalpy of formation tends to be less exothermic monotonically as the mole fraction of calcium or average ionic potential increases, showing decreased stability. For samples with the same chemical composition, their enthalpies of formation become more exothermic in the sequence of anhydrous zeolite (AZ), amorphous (AP) and dense phase (DP), indicating increasing thermodynamic stability and providing the thermodynamic driving force for the transformations.

Acknowledgements

H.S. is grateful to the National Natural Science Foundation of China for the financial support under the National Natural Science Fund for Young Scholar (No. 21201063), the Ministry of Education of Republic of China for the financial support under the Research Fund for the Doctoral Program of Higher Education of China (RFDP) (No. 20110074120020) and the Fundamental Research Funds for the Central Universities, and the China Scholarship Council for the State Scholarship Fund (No. 201308310077). The calorimetric work at UC Davis was supported by the U.S. Department of Energy, Office of Basic Energy Sciences, grant DEFG02-97ER14749.

Notes

[a] State Key Laboratory of Chemical Engineering, East China University of Science and Technology, Shanghai 200237, P. R. China.
[b] Peter A. Rock Thermochemistry Laboratory and NEAT ORU, University of California, Davis, California, 95616, USA.

†H.S., D.W. and A.N. designed the research. H.S., D.W. and X.G. performed the experiments. H.S. D.W., X.G. and A.N. analyzed the data. H.S. D.W. and A.N. wrote the paper.

Electronic Supplementary Information (ESI) available: See DOI: 10.1039/b000000x/

References

1. N. Y. Chen, Gorwood, W.E., Dwyer, F.G., Shape selective catalysis in industrial applications, Macel Dekker, Inc., New York, 1996.
2. J. Weitkamp and L. Puppe, Catalysis and zeolites : fundamentals and applications, Springer, Heidelberg, 1999.
3. S. M. Auerbach, Carrado, K.A., Dutta, P.K., Handbook of Zeolite Science and Technology, Taylor & Francis, London, 2003.
4. S. Kulprathipanja, Zeolites in Industrial Separation and Catalysis, WILEY-VCH Verlag GmbH & Co. KGaA, Weinheim, 2010.
5. J. M. Newsam, J Phys Chem-Us, 1988, 92, 445-452.
6. V. Dondur, N. Petranovic and R. Dimitrijevic, Mater Sci Forum, 1996, 214, 91-98.
7. V. Kahlenberg and H. Bohm, Am Mineral, 1998, 83, 631-637.
8. W. Lutz, B. Fahlke, U. Lohse and R. Seidel, Chem Tech-Leipzig, 1983, 35, 250-253.
9. R. Dimitrijevic, V. Dondur and A. Kremenovic, Zeolites, 1996, 16, 294-300.
10. C. Kosanovic, B. Subotic and I. Smit, Thermochim Acta, 1998, 317, 25-37.
11. A. Navrotsky, Nat Mater, 2003, 2, 571-572.
12. R. Dimitrijevic, V. Dondur, P. Vulic, S. Markovic and S. Macura, J Phys Chem Solids, 2004, 65, 1623-1633.
13. K. Selvaraj, Micropor Mesopor Mat, 2010, 135, 82-89.
14. A. S. Pakhomova, R. M. Danisi, T. Armbruster, B. Lazic, F. Gfeller, S. V. Krivovichev and V. N. Yakovenchuk, Micropor Mesopor Mat, 2013, 182, 207-219.
15. F. E. Trigueiro, D. F. J. Monteiro, F. M. Z. Zotin and E. F. Sousa-Aguiar, J Alloy Compd, 2002, 344, 337-341.
16. P. Castaldi, L. Santona, C. Cozza, V. Giuliano, C. Abbruzzese, V. Nastro and P. Melis, J Mol Struct, 2005, 734, 99-105.
17. A. Radulovic, V. Dondur, R. Dimitrijevic and D. Arandjelovic, Thermochim Acta, 2010, 511, 37-42.
18. A. Radulovic, V. Dondur, P. Vulic, Z. Miladinovic, G. Ciric-Marjanovic and R. Dimitrijevic, J Phys Chem Solids, 2013, 74, 1212-1220.
19. F. A. Da Silva and A. E. Rodrigues, Ind Eng Chem Res, 2001, 40, 5758-5774.
20. X. J. Yin, G. S. Zhu, W. S. Yang, Y. S. Li, G. Q. Zhu, R. Xu, J. Y. Sun, S. L. Qiu and R. R. Xu, Adv Mater, 2005, 17, 2006-2010.
21. J. A. Silva and A. E. Rodrigues, Sep Purif Technol, 1998, 13, 195-208.
22. P. E. Riley and K. Seff, Journal of Physical Chemistry, 1975, 79, 1594-1601.
23. C. Kosanovic, B. Subotic and A. Ristic, Mater Chem Phys, 2004, 86, 390-398.
24. C. Kosanovic, B. Subotic and E. Kranjc, Micropor Mesopor Mat, 2004, 71, 27-32.
25. A. Navrotsky, Phys Chem Miner, 1977, 2, 89-104.
26. A. Navrotsky, Phys Chem Miner, 1997, 24, 222-241.
27. T. Ohgushi, K. Ishimaru and S. Komarneni, J Am Ceram Soc, 2001, 84, 321-327.
28. D. W. H. Sun, X.F. Guo, B.X. Shen, A. Navrotsky., Submitted manuscript, 2014.
29. A. Navrotsky and Z. R. Tian, Chem-Eur J, 2001, 7, 769-774.
30. O. Trofymluk, A. A. Levchenko and A. Navrotsky, Micropor Mesopor Mat, 2012, 149, 119-125.
31. V. J. Hall and G. J. Simpson, J Am Chem Soc, 2010, 132, 13598-13599.
32. J. W. Morse and W. H. Casey, Am J Sci, 1988, 288, 537-560.
33. B. N. Roy and A. Navrotsky, J Am Ceram Soc, 1984, 67, 606-610.
34. I. Kiseleva, A. Navrotsky, I. A. Belitsky and B. A. Fursenko, Am Mineral, 1996, 81, 658-667.